J. Fluid Mech. (2002), *vol.* 470, *pp.* 269–290.
DOI: 10.1017/S0022112002001933 Printed in the United Kingdom

The interactive dynamics of flow and directional solidification in a Hele-Shaw cell Part 2. Stability analysis and nonlinear simulations

By SUDHIR S. BUDDHAVARAPU AND ECKART MEIBURG†

Department of Aerospace and Mechanical Engineering, University of Southern California, Los Angeles, CA 90089-1191, USA

(Received 9 May 2001 and in revised form 8 April 2002)

A linear stability analysis as well as nonlinear simulations are performed in order to analyse the coupling between the directional solidification of a binary alloy and the flow in its melt. An incompressible, potential flow model is assumed, whose validity is tested through comparisons with the accompanying experiments of Zhang & Maxworthy (2002) in a Hele-Shaw cell. The linear stability analysis predicts that a uniform flow parallel to the interface reduces the growth rates of directional solidification instabilities. In addition, the dominant wavelength is shifted to larger values by the flow, and a small propagation velocity in the downstream direction is observed. These findings are confirmed by the nonlinear simulations as well. While the overall stabilization is confirmed by the experiments, the predicted values of the dominant wavenumber and its growth rate are too high by factors of two and four, respectively. These differences are attributed to the existence of a velocity boundary layer in the melt, which strongly affects the lateral solute transport.

1. Introduction

In part 1 of this work (Zhang & Maxworthy 2002), the effect of a uniform parallel flow on a directional solidification process in a Hele-Shaw cell is analysed experimentally. The authors observe that such flows in general reduce the growth rate of the interfacial instability, without noticeably altering the dominant wavelength. While the experimental data do not suggest a substantial propagation velocity of the perturbations as a result of the externally imposed flow, the growing cells are seen to tilt against the direction of the flow once they reach large amplitudes. The present analysis complements part 1, in that it focuses on the linear stability behaviour of a directionally solidifying interface in the presence of a Hele-Shaw flow, and it also presents some simulation results for the early nonlinear phase.

As can be seen from the literature survey given in part 1, the present experimental and computational investigation represents a further step in the ongoing effort to understand the coupling mechanisms between the solidification process and convective flow in the melt. From the early stability analysis of Mullins & Sekerka (1964) it

† Author to whom correspondence should be addressed. Present address: Department of Mechanical and Environmental Engineering, University of California, Santa Barbara, CA 93106, USA.

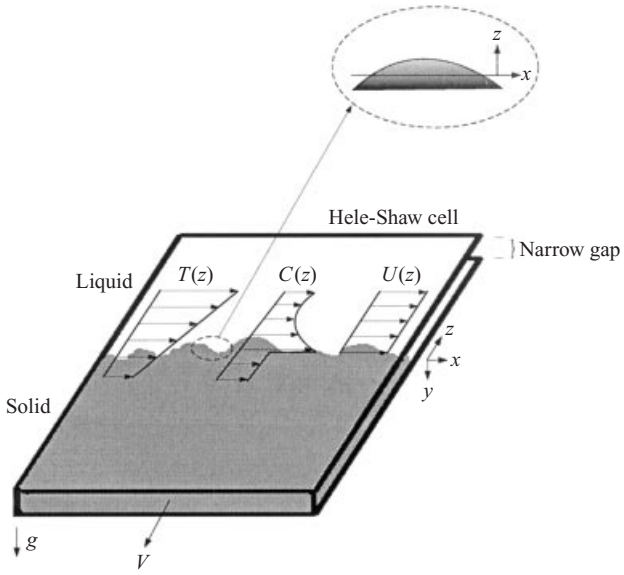

FIGURE 1. Sketch of the problem under consideration. A Hele-Shaw cell containing a binary alloy is pulled against the direction of an externally imposed temperature gradient. The preferential rejection of solute at the solidifying interface sets up a concentration boundary layer, which can give rise to an instability of the solidification process. The effect of a nominally uniform flow parallel to the interface on the solidification process is to be analysed.

was realized that such an understanding is essential in order to design processes for growing high-quality crystals from binary melts. Hurle (1969, 1977) and Delves (1968, 1971) describe early investigations into the coupling of flow and solidification. More recently, the effects of a variety of externally imposed flow fields on the stability of the solidifying interface have been analysed in great detail. Coriell *et al.* (1984) perform a linear stability analysis in the presence of a Couette flow, while Forth & Wheeler (1989, 1992) focus on the effects of an asymptotic suction profile. Davis and colleagues analyse the effects of time-dependent, stagnation-point and various other flow features (Brattkus & Davis 1988*a*, *b*; Schulze & Davis 1994, 1995, 1996). The coupling of morphological instabilities with cellular convection is addressed by Bühler & Davis (1998), Caroli *et al.* (1985*a*, *b*), Dantzig & Chao (1986, 1990) and Chen & Davis (1999). More recently, the effects of flow on fully developed dendrites have been investigated computationally by Tong, Beckermann & Karma (2000), Tonhardt & Amberg (1998, 2000). Comprehensive reviews of the field are provided by Sekerka (1968) and Glicksman, Coriell & McFadden (1986) and Davis (1990, 1993).

In the present investigation, we focus on an externally imposed uniform flow parallel to the solidifying interface. Section 2 describes the physical problem along with the governing equations. In § 3, the linear stability analysis is performed and the results discussed. Section 4 focuses on nonlinear simulations for the early stages of the solidification process. In addition to the uniform parallel flow, the effects of a source/sink combination are discussed as well. Finally, § 5 summarizes the findings and presents conclusions.

2. Physical problem and governing equations

We consider the solidification process of a binary alloy between two closely spaced, horizontal plates forming a Hele-Shaw cell, as shown in figure 1. The gap is assumed

to be sufficiently narrow to suppress any buoyancy-driven convection. The entire Hele-Shaw cell moves with constant velocity V in the $-z$-direction, through an externally imposed temperature field $T(z)$ with constant gradient. The solid/melt interface extends along the x-direction. If the solidification process takes place in a stable fashion, a steady state will be reached in which the interface remains stationary in a laboratory reference frame, at the location where the temperature equals the solidification temperature. However, it is well known on the basis of both linear stability theory (Mullins & Sekerka 1964) and experimental investigations (e.g. Rutter & Chalmers 1953; Boettinger *et al.* 1984; Trivedi, Sekhar & Seetharaman 1989) that preferential rejection of solute at the interface can result in a concentration boundary layer that renders the solidification process unstable if a critical pulling velocity V_c is exceeded. In the absence of flow in the melt, this instability is referred to as pure morphological instability. The purpose of the present investigation is to quantify the effects of a uniform flow of strength U_∞ parallel to the interface on the instability.

The investigation will be based on the set of gap-averaged, two-dimensional equations as formulated by Davis (1990). In the laboratory reference frame, the concentration field in the melt is governed by the convective–diffusive equation

$$c_t + (\boldsymbol{u} \cdot \nabla)c - Vc_z = D\nabla^2 c, \tag{2.1}$$

where the velocity field in the melt is assumed to be incompressible and irrotational in nature:

$$\boldsymbol{u} = \nabla\phi, \tag{2.2}$$

$$\nabla^2\phi = 0. \tag{2.3}$$

Obviously, the potential flow approach precludes us from imposing a no-slip condition at the interface, and from resolving the corresponding velocity boundary layer, whose thickness is of the order of the gap width of the Hele-Shaw cell. The question arises as to whether Taylor dispersion effects may be important regarding the evolution of the concentration field within the narrow gap of the Hele-Shaw cell (Petitjeans *et al.* 1999). However, for the gap width, maximum flow velocity and molecular diffusivity employed in part 1, an estimate based on the analysis by Horne and Rodriguez (1983) shows the Taylor dispersion coefficient to be roughly two orders of magnitude smaller than the molecular diffusion coefficient. As a result, the effects of Taylor dispersion can safely be neglected in the present investigation. By assuming that (i) the thermal diffusivity is much larger than the diffusion coefficient of the solute, (ii) the thermal diffusion coefficients of the solid and the melt are identical, and (iii) the accumulation of latent heat L at the interface is negligible, we can apply the frozen temperature approximation (Langer 1980)

$$T = T_0 + Gz. \tag{2.4}$$

Here G represents the externally applied temperature gradient, and T_0 indicates an arbitrary reference temperature. Thermodynamics states that the temperature T_I at the interface varies with the slope m of the liquidus line in the phase diagram according to

$$T_I = mc^+ + T_M\left(1 + 2H\frac{\gamma}{L}\right), \tag{2.5}$$

where T_M is the melting temperature of a planar interface of pure solid, γ denotes the surface energy, while H represents the local interfacial curvature

$$H = \tfrac{1}{2}\nabla \cdot [(1 + |\nabla h|^2)^{-1/2}\,\nabla h]. \tag{2.6}$$

By combining equations (2.4), (2.5) and (2.6), one obtains

$$T_0 - T_M + Gh = mc^+ + T_M \frac{\gamma}{L} 2H. \tag{2.7}$$

The solute balance across the interface is

$$(1-k)c^+(V + h_t) = -D(c_z^+ - c_x^+ h_x), \tag{2.8}$$

where c^+ and c^- denote the concentration values on the liquid and solid sides of the interface, respectively. This discontinuity in the concentration field across the interface is caused by preferential rejection, which can be quantified by the segregation coefficient k,

$$k = \frac{c^-}{c^+}. \tag{2.9}$$

As boundary condition for the velocity field at the solid/melt interface, we have

$$\frac{\phi_z}{\phi_x} = h_x. \tag{2.10}$$

In addition, far away from the interface, we apply

$$\phi_z \to 0. \tag{2.11}$$

The entire problem is considered to be periodic in the spanwise x-direction. In order to render the above equations and boundary conditions dimensionless, we introduce characteristic scales for length (D/V), velocity (V), time (D/V^2), temperature (GD/V) and concentration ($c_\infty(1-k)/k$). In this way, we obtain the dimensionless equations as

$$c_t + uc_x + wc_z - c_z = c_{xx} + c_{zz}, \tag{2.12}$$

$$h_t = -\frac{c_z - h_x c_x}{(1-k)c^+ + 1} - 1, \tag{2.13}$$

$$c|_{z=h} = c^+ = -\frac{1}{M}h + RH, \tag{2.14}$$

$$H = \frac{1}{2}\frac{h_{xx}}{[1+h_x^2]^{3/2}}, \tag{2.15}$$

$$c|_{z\to\infty} = -1, \tag{2.16}$$

$$\nabla^2 \phi = 0. \tag{2.17}$$

In addition to the dimensionless parameters k and U ($U = U_\infty/V$), we thus obtain

$$M = \frac{m(k-1)}{k}\frac{c_\infty V}{DG} = \frac{mG_c}{G}, \tag{2.18}$$

$$R = -\frac{2T_M \gamma V k}{mLDc_\infty(1-k)}. \tag{2.19}$$

M indicates the ratio of the destabilizing concentration gradient at the interface to the stabilizing externally imposed temperature gradient, and R provides a dimensionless value of the stabilizing surface energy parameter. Note that in part 1 a dimensionless surface energy parameter is employed which is different from the present one by a constant factor.

3. Linear stability analysis

In the following, we will investigate the linear stability of the solid/melt interface in the presence of a uniform flow in the x-direction with dimensionless velocity U. The stationary base state is given by

$$\bar{h}(x) = 0, \tag{3.1}$$

$$\bar{\Phi}(x) = Ux, \tag{3.2}$$

$$\bar{c}(z) = \mathrm{e}^{-z} - 1. \tag{3.3}$$

We assume wavy perturbations of the shape

$$h(x,t) = h_o\,\mathrm{e}^{\mathrm{i}\omega(x-qt)}, \tag{3.4}$$

$$\phi(x,z,t) = \varphi(z)\,\mathrm{e}^{\mathrm{i}\omega(x-qt)}, \tag{3.5}$$

$$c(x,z,t) = B(z)\,\mathrm{e}^{\mathrm{i}\omega(x-qt)}, \tag{3.6}$$

where $\omega = 2\pi/\lambda$ is the real wavenumber, $q = q_r + \mathrm{i}q_i$ denotes the complex wave velocity, and $B(z)$ and $\varphi(z)$ represent the complex eigenfunctions of the concentration and velocity potential perturbations, respectively. The perturbations grow at the rate $\sigma = \omega q_i$. After substituting the above form of the perturbations into the governing equations, subtracting out the base state, and linearizing, we obtain eigenfunctions of the form

$$\varphi(z) = -\mathrm{i}Uh_o\,\mathrm{e}^{-\omega z}, \tag{3.7}$$

$$B(z) = [\hat{Q}\,\mathrm{e}^{-(1+\omega)z} + A\,\mathrm{e}^{\lambda z}], \tag{3.8}$$

where

$$\lambda = -\tfrac{1}{2} - \tfrac{1}{2}\sqrt{1 + 4\omega^2 + 4\mathrm{i}\omega U - 4\mathrm{i}\omega q}. \tag{3.9}$$

The above shape of the eigenfunctions shows that the perturbation velocity field in the direction tangential to the interface is in phase with the interfacial deformation: it reaches a maximum above the crests, and a minimum in the valleys. On the other hand, $\hat{Q}$ is a complex quantity, so that the perturbation concentration field is shifted in the streamwise direction with respect to the interfacial deformation. This leads us to expect the existence of waves travelling along the interface. By eliminating $\varphi(z)$, we obtain

$$\begin{aligned}\frac{1-k}{k}c_\infty[\omega q_i - \mathrm{i}\omega q_r] + (1-k)\left[\frac{G}{m} + \frac{T_M\gamma}{Lm}\omega^2\right] \\ = G_c + \left[\left(\frac{G - mG_c}{m} + \frac{T_M\gamma}{Lm}\omega^2 - \hat{Q}_r - \mathrm{i}\hat{Q}_i\right)\Delta + (\hat{Q}_r + i\hat{Q}_\mathrm{i})(1+\omega)\right],\end{aligned} \tag{3.10}$$

with

$$\Delta = \tfrac{1}{2} + \tfrac{1}{2}\sqrt{1 + 4\omega^2 + 4\omega q_i + \mathrm{i}4\omega(U - q_r)}, \tag{3.11}$$

$$\frac{\hat{Q}_r}{G_c} = -\frac{1}{1 + [(q_i - 1)/(q_r - U)]^2}, \tag{3.12}$$

$$\frac{\hat{Q}_i}{G_c} = \frac{(q_i - 1)/(q_r - U)}{1 + [(q_i - 1)/(q_r - U)]^2}. \tag{3.13}$$

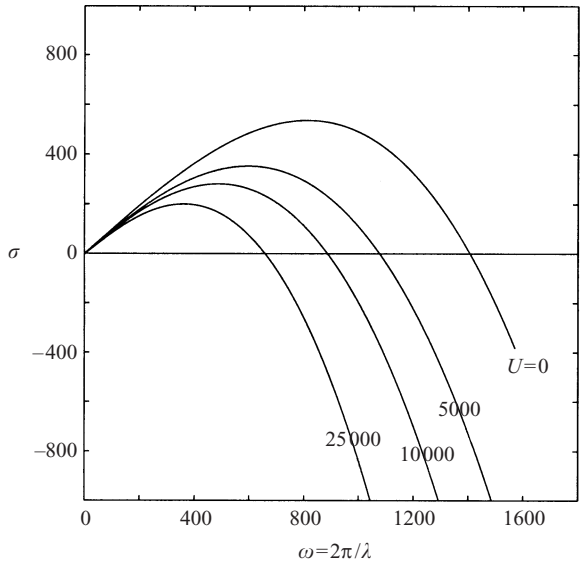

FIGURE 2. Linear stability analysis: the effect of the uniform flow velocity U on the growth rate for $M = 100$, $k = 0.1$ and $R = 10^{-6}$. Increasing values of U are seen to be stabilizing.

After further algebraic manipulation, we arrive at the eigenvalue problem

$$F \equiv \Re + \mathrm{i}\Im = 0, \tag{3.14}$$

$$\Re = 2\left[(1-k)\left\{\frac{1}{M} + \frac{R\omega^2}{2}\right\} - \omega q_i - (1+\omega)\frac{\hat{Q}_r}{G_c}\right] - \left\{\frac{1-M}{M} + \frac{R\omega^2}{2} - \frac{\hat{Q}_r}{G_c}\right\}\left(1 + \sqrt{r}\cos\frac{\theta}{2}\right) - \frac{\hat{Q}_i}{G_c}\sqrt{r}\sin\frac{\theta}{2}, \tag{3.15}$$

$$\Im = 2\left[\omega q_r - (1+\omega)\frac{\hat{Q}_i}{G_c}\right] + \frac{\hat{Q}_i}{G_c}\left(1 + \sqrt{r}\cos\frac{\theta}{2}\right) - \left\{\frac{1-M}{M} + \frac{R\omega^2}{2} - \frac{\hat{Q}_r}{G_c}\right\}\sqrt{r}\sin\frac{\theta}{2}, \tag{3.16}$$

where

$$r = \sqrt{(1 + 4\omega^2 + 4\omega q_i)^2 + 4\omega(U - q_r)^2}, \tag{3.17}$$

$$\theta = \arctan\left[\frac{4\omega(U - q_r)}{1 + 4\omega^2 + 4\omega q_i}\right]. \tag{3.18}$$

Equation (3.14) can be solved iteratively to obtain q_r and q_i as functions of ω for different values of the governing parameters.

Figure 2 shows the dispersion relations for different values of the dimensionless mean velocity U, $M = 100$, $k = 0.1$ and $R = 10^{-6}$, which represent typical parameter values encountered in the accompanying experiments of part 1. It should be pointed out that, in the absence of flow, the data agree with the earlier results by Mullins & Sekerka (1964) on the pure morphological instability. The graph demonstrates

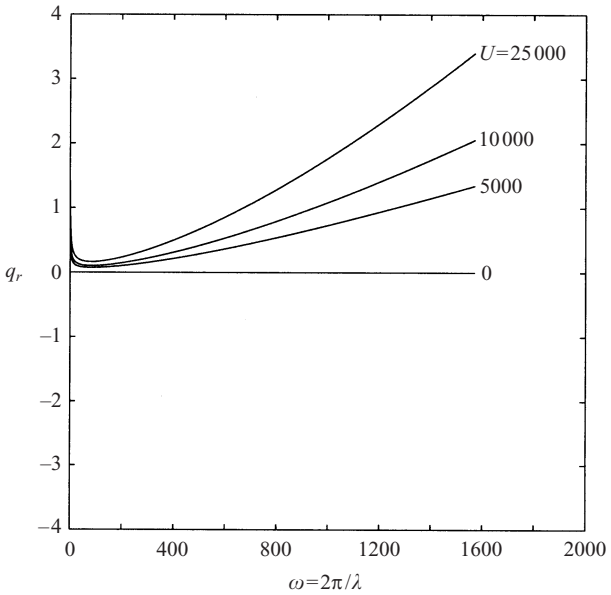

FIGURE 3. Linear stability analysis: the effect of the uniform flow velocity U on the propagation velocities of perturbation waves for $M = 100$, $k = 0.1$ and $R = 10^{-6}$. The interfacial waves travel in the direction of the externally imposed flow, at velocities two to four orders of magnitude smaller than the flow. For each value of U, a minimum of the propagation velocity is observed at an intermediate wavenumber.

that an increase in the strength of the mean flow will reduce the growth rate of all wavenumbers. This behaviour is similar to the results obtained by Coriell *et al.* (1984) and Forth & Wheeler (1989) for Couette and boundary-layer-like viscous shear flows in the melt. Both of these investigations show a stabilization of the morphological instability by the forced shear flow in the melt, with respect to perturbations whose wave vector is parallel to the flow. On the other hand, perturbations with wave vectors perpendicular to the flow are unaffected by it. Interestingly, the investigation of Coriell *et al.* (1984) shows that increasing shear leads to shorter wavelengths at the onset of instability, while figure 2 demonstrates a shift to longer wavelengths for increasing values of U.

Figure 3 shows the predicted values of q_r for the same values of U. Clearly the propagation velocity depends on the wavenumber, as well as on the strength of the imposed flow. For all combinations of U, R and M, we find the waves to travel in the *downstream* direction with a velocity roughly two to four orders of magnitude less than that of the mean flow. In general, for a given wavenumber, the propagation velocity increases with U. This observation resembles the findings of Coriell *et al.* (1984), who show that a forced Couette flow leads to the appearance of waves travelling in the downstream direction, with a velocity that increases with the shear. Forth & Wheeler (1989), on the other hand, find that a suction-type boundary layer profile can result in either upstream or downstream travelling waves.

Interestingly, figure 3 shows that for a given value of U there is an intermediate wavenumber for which the propagation velocity has a minimum. Closer inspection of the results shows that this wavenumber of minimum propagation velocity initially drops with increasing values of U, before reaching an asymptotic plateau around

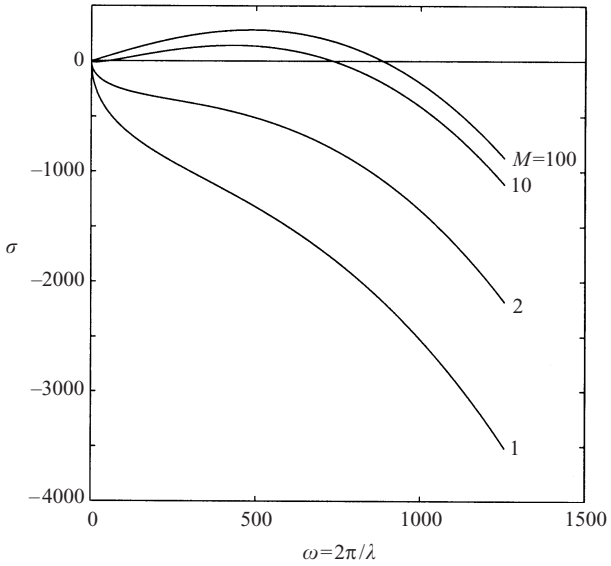

FIGURE 4. Linear stability analysis: the effect of the stability parameter M on the growth rate for $U = 10^4$, $k = 0.1$ and $R = 10^{-6}$. As for the case without flow, increasing the value of M leads to a destabilization of the solidification process.

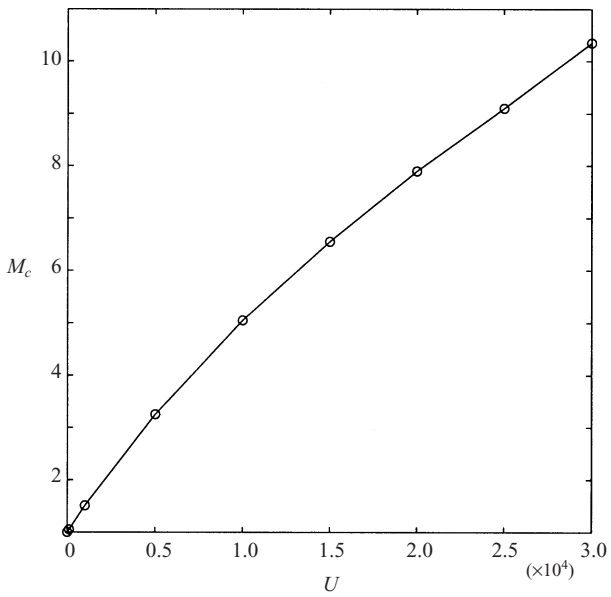

FIGURE 5. Linear stability analysis: the dependence of the critical morphological number M_c on the strength U of the externally imposed uniform flow for $k = 0.1$ and $R = 10^{-6}$. M_c grows approximately linearly with U.

$U = 10^4$. The propagation velocity of this wavenumber keeps increasing, however, without showing any signs of saturation.

In order to investigate the effect of the stability parameter M on the dispersion relationship in the presence of an externally imposed uniform flow, we focus on the above parameter values for R and k, along with $U = 10^4$. We observe that there exists

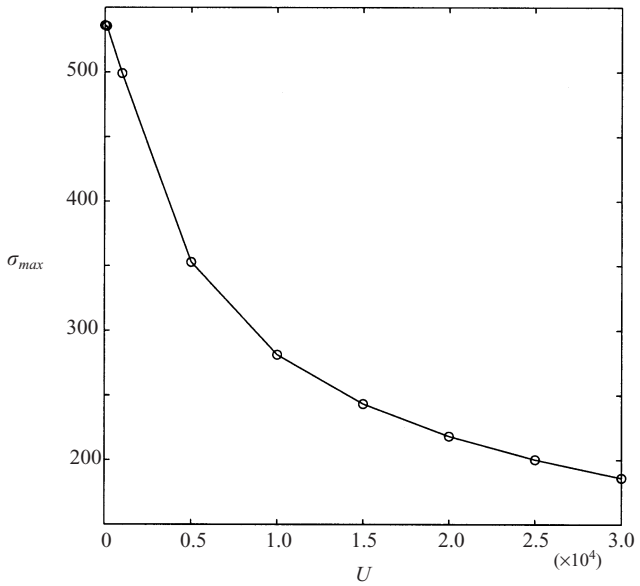

FIGURE 6. Linear stability analysis: the effect of the externally imposed flow velocity U on the maximum growth rate for $M = 100$, $k = 0.1$ and $R = 10^{-6}$. Increasing flow velocities are seen to reduce the maximum growth rates.

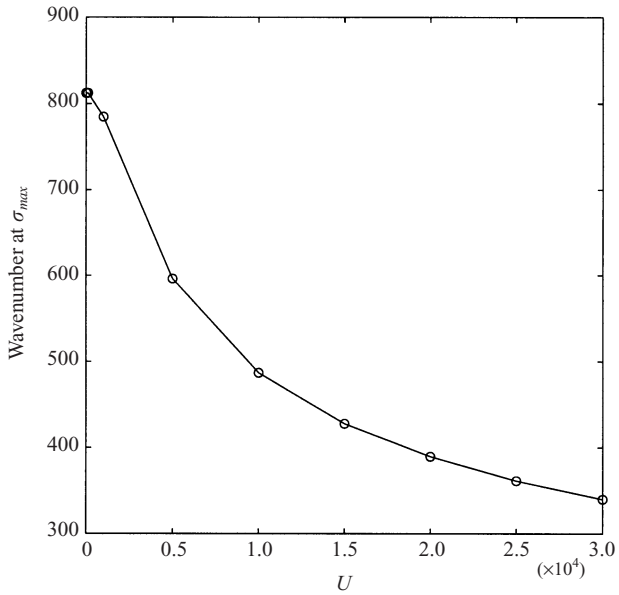

FIGURE 7. Linear stability analysis: the effect of the externally imposed flow velocity U on the wavenumber of the most amplified perturbation for $M = 100$, $k = 0.1$ and $R = 10^{-6}$. Increasing values of U shift the peak amplification towards longer waves.

a critical morphological number (M_c) below which the interface remains stable to perturbations of all wavenumbers, cf. figure 4. By computing M_c for different values of U, we find that M_c increases monotonically with U for the given values of R and k, cf. figure 5. The data indicate an approximately tenfold increase of the critical value for velocities around 3×10^4.

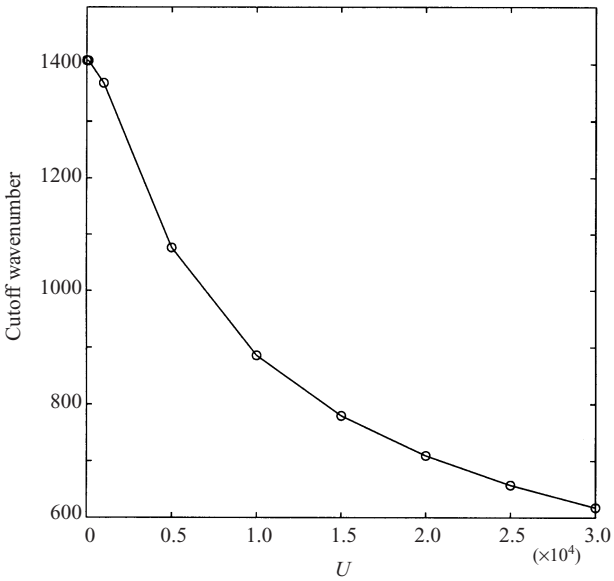

FIGURE 8. Linear stability analysis: the effect of the externally imposed flow velocity U on the cutoff wavenumber for $M = 100$, $k = 0.1$ and $R = 10^{-6}$. Increasing values of U narrow the range of unstable perturbation modes.

Figure 6 displays the effect of U on the maximum growth rate for the same parameter combination as above. Increasing values of U are seen to uniformly reduce the growth rate, i.e. to render the solidification process less unstable. At the same time, increasing U leads to a reduction in both the most amplified wavenumber (figure 7) and the cutoff wavenumber (figure 8).

In order to evaluate the influence of the surface energy parameter on the linear stability, R was varied between 10^{-6} and 2×10^{-4}, for $M = 100$ and $k = 0.1$. We find that for relatively weak imposed flows such as $U = 100$, R has a negligible effect on the dispersion relation. For stronger flows, however, the influence of R is more substantial. Larger values of R are seen to reduce the growth rates and to reduce the range of unstable wavenumbers, cf. figure 9.

Figure 10 displays the effect of R on the propagation velocity. The dashed line, which intersects each parametric curve $R = \text{const.}$ at the cutoff wavenumber, divides the figure into an unstable and a stable region. Higher values of R are seen to result both in a narrower range of unstable wavenumbers and in larger propagation velocities. It should be pointed out that in the experiments in part 1, R is in the range $10^{-6} \sim 10^{-5}$. The linear stability results show very small propagation velocities in this range.

The physical mechanism behind the stabilization by the uniform flow parallel to the interface is straightforward to recognize. As has been mentioned by several authors before, e.g. Davis (1990), in the absence of flow excess solute accumulates in the troughs of the wavy interface perturbations. In this way, the concentration gradient in the melt at the interface is weakest in the trough and steepest at the crest. This results in the faster (slower) growth of the crests (troughs), thereby leading to the instability. The imposed flow parallel to the boundary now has the effect of transporting solute-rich fluid from the troughs to the crests (figure 11). Simultaneously it carries solute-impoverished fluid from the crests to the troughs. Overall it thus

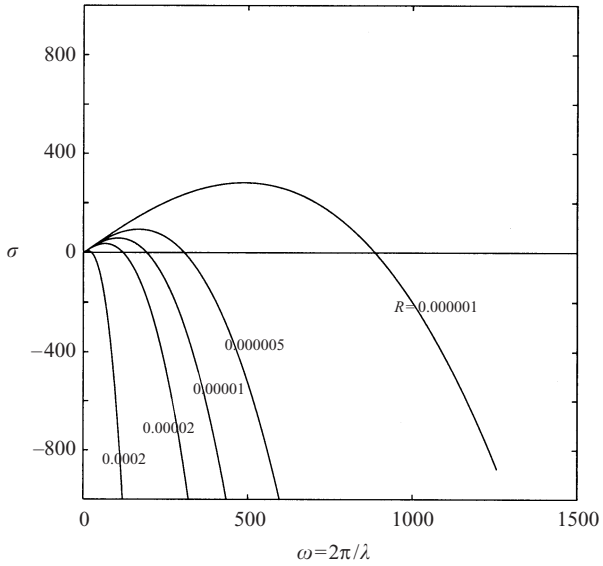

FIGURE 9. Linear stability analysis: the effect of the surface energy parameter R on the dispersion relation for $M = 100$, $k = 0.1$ and $U = 10^4$. Increasing values of R are seen to be uniformly stabilizing.

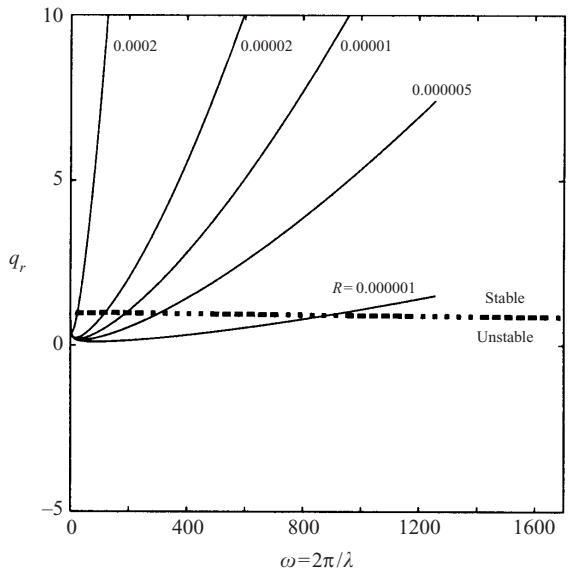

FIGURE 10. Linear stability analysis: the effect of the surface energy parameter R on the propagation velocity for $M = 100$, $k = 0.1$ and $U = 10^4$. Increasing values of R result in larger propagation velocities. The dashed line divides the plane into a stable and an unstable parameter range.

renders the solute concentration gradient near the interface more uniform, which leads to enhanced stability.

The effect on the wave propagation velocity can be explained in a similar fashion. On the windward side of the crest, the potential flow shifts the weaker concentration gradient up the slope, thus rendering this region more stable. On the other hand, the

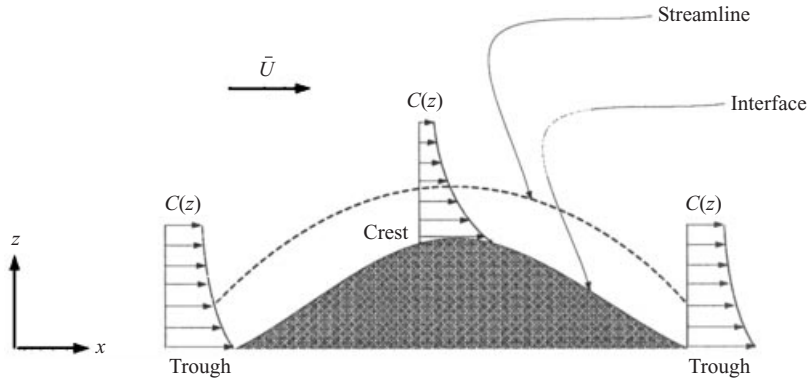

FIGURE 11. The physical mechanism behind the stabilization by a uniform flow parallel to the interface. The milder concentration gradients forming in the troughs without flow are convected towards the crests by the flow, prompting them to grow more slowly. Conversely, the steeper concentration profiles that would evolve near the crests without flow, are brought closer to the troughs by the external flow, thereby accelerating their growth.

leeward side experiences a lateral shift of the steeper concentration gradient down the slope, which destabilizes it. In this fashion, a travelling wave in the direction of the mean flow is generated.

4. Nonlinear simulations

4.1. *Numerical technique*

In order to investigate the nonlinear interaction of the unstable interface with the externally imposed flow, we focus on a physical domain of size $L_x \times L_z$. Consistent with the stability analysis, we assume the problem to be periodic in the spanwise x-direction. This allows us to employ a Fourier spectral technique in the x-direction, so that we can decompose the interfacial boundary as

$$h(x,t) = \sum_{n=-N}^{N} a_n(t)\, \mathrm{e}^{-\mathrm{i}2\pi n\xi}, \tag{4.1}$$

where $a_n(t) = a_{n_r}(t) + \mathrm{i}a_{n_i}(t)$ represent the time-dependent complex Fourier coefficients. We map the physical domain $0 < x < L_x$, $h < z < L_z$ into the computational domain $0 < \xi < 1$, $0 < \eta < 1$:

$$x(\xi,\eta,t) = L_x\xi, \tag{4.2}$$

$$z(\xi,\eta,t) = L_z\eta + (1-\eta)\sum_{n=-N}^{N} a_n\, \mathrm{e}^{-\mathrm{i}2\pi n\xi}. \tag{4.3}$$

Note that this mapping will not allow us to simulate configurations in which $h(x)$ is not single-valued, so that we have to terminate the simulations before this would occur. One arrives at the following transformed equations:

$$c_t = -\frac{u}{Pe}c_\xi + [\eta_{xx} + (1-w)\eta_z - u\eta_x - \eta_t]c_\eta + \frac{1}{Pe^2}c_{\xi\xi} + [{\eta_x}^2 + {\eta_z}^2]c_{\eta\eta} + \frac{2}{Pe}\eta_x c_{\xi\eta}, \tag{4.4}$$

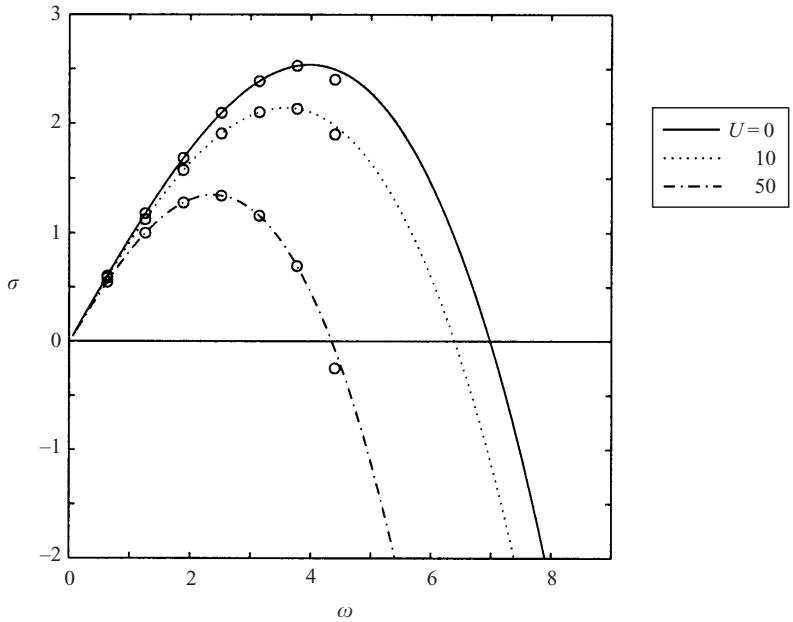

FIGURE 12. Validation of the nonlinear code. The growth rates of prescribed small perturbations in the numerical simulations (circles) are compared with those obtained from linear stability theory (lines) for $M = 100$, $k = 0.1$, $R = 0.04$, as well as $U = 0$, 10 and 50.

$$h_t = -\frac{\eta_z c_\eta - Pe^{-2} h_\xi c_\xi - Pe^{-1} \eta_x h_\xi c_\eta}{(1-k)c^+ + 1} - 1, \tag{4.5}$$

$$c|_{\eta=0} = c^+ = -\frac{1}{M} h + RH, \tag{4.6}$$

$$H = \frac{1}{2} \frac{Pe^{-2} h_{\xi\xi}}{[1 + (Pe^{-1} h_\xi)^2]^{3/2}}, \tag{4.7}$$

$$c|_{\eta=1} = \mathrm{e}^{-PeA} - 1. \tag{4.8}$$

Here $Pe = VL_x/D$ denotes the Péclet number formed with the length of the computational domain in the direction parallel to the interface. $A = L_z/L_x$ represents the aspect ratio of the computational domain. The above equations are discretized by means of a Fourier spectral technique (Gottlieb & Orszag 1977) in the periodic direction, and a compact finite difference method (Lele 1992) in the pulling direction. The latter is of sixth-order accuracy in the interior, and of third-order near the boundaries. The equations are advanced in time by means of a third-order Runge–Kutta scheme (Wray 1991). The potential velocity field is represented by a boundary element technique (Anderson 1991), which places source and sink panels of varying strength along the boundary in order to satisfy the condition of vanishing normal velocity. In order to satisfy the periodic boundary conditions, several mirror images of the sources and sinks in the x-direction are taken into account when evaluating the velocity field.

4.2. *Validation*

In order to validate the code, we performed simulations for individual wavy perturbations of small amplitude (10^{-5}), whose growth rates and propagation velocities could

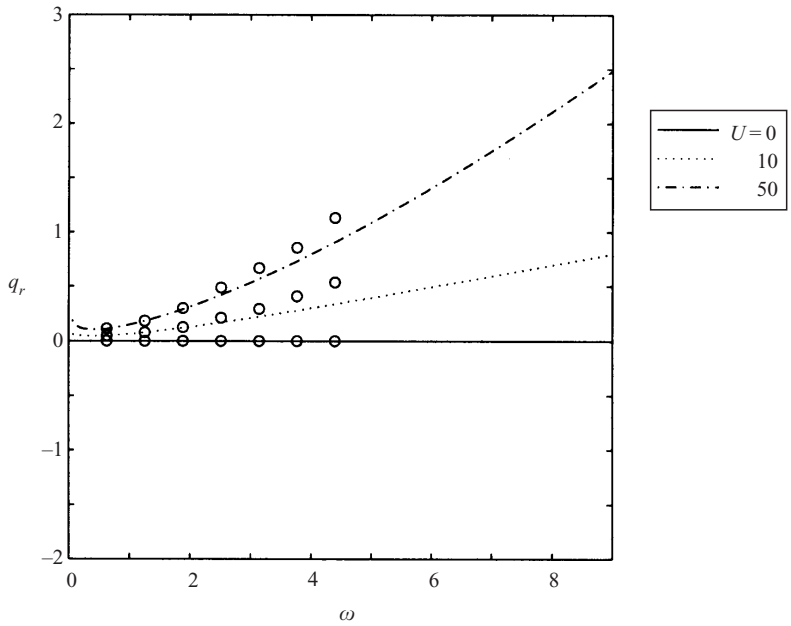

FIGURE 13. Validation of the nonlinear code. The propagation velocities of small perturbations in the numerical simulations (circles) are compared with those obtained from linear stability theory (lines) for $M = 100$, $k = 0.1$, $R = 0.04$, as well as $U = 0$, 10 and 50.

then be compared with the results from linear stability theory. For a discretization of 16×129 points in the x- and z-directions, respectively, the results are shown in figures 12 and 13 for a parameter combination of $R = 0.04$, $M = 100$ and $k = 0.1$, as well as imposed parallel velocities of $U = 0$, 10 and 50. The agreement is very good with respect to the growth rates. For the relatively coarse discretization of the validation simulations, the predicted propagation velocity is slightly too high.

4.3. *Results*

4.3.1. *Uniform parallel flow*

In order to investigate the nonlinear growth of the interfacial instability, we initially impose perturbations corresponding to the first five modes, each with an amplitude of 10^{-3} and a random phase. The resulting initial condition for the interfacial shape is shown in figure 14. For the governing dimensionless parameter values of $M = 100$, $k = 0.1$ and $R = 0.04$, the no-flow case will be compared with the uniform flow case of $U = 50$. Note that, while the values of M and k are comparable to those in the experiments part 1, we are forced to employ a larger value of R for reasons of numerical resolution. The computational domain size is given by $L_x = 10$ and $L_z = 20$. To allow better comparisons, the initial perturbation is exactly the same for the no-flow case and for the externally imposed flow case of $U = 50$.

For $U = 0$, figures 15 and 16 display the temporal growth of the interfacial perturbation, as well as the overall concentration field at the final time $t = 2.13$. It is interesting to note that the final interfacial shape has six maxima, even though the initial interfacial perturbation contained only five of them. This evolution is in good agreement with linear stability theory, which predicts modes six and seven to be the fastest growing ones. Note that the solute rejected within the troughs becomes trapped, thereby leading to locally weak concentration gradients. On the other hand,

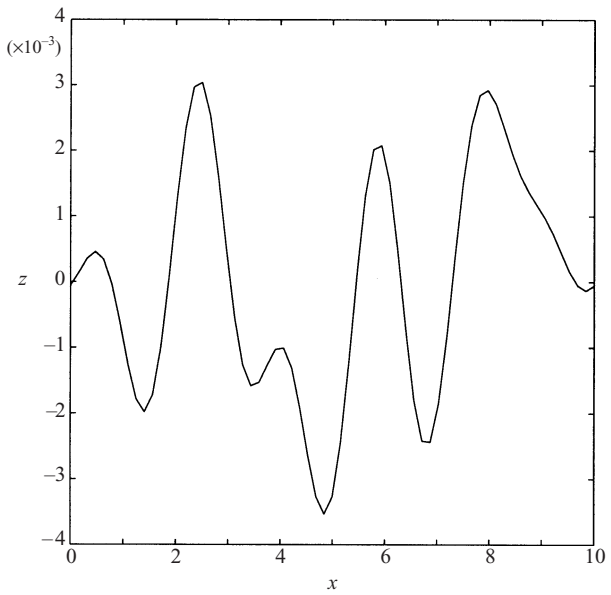

FIGURE 14. Initial condition for the solid/melt interfacial shape in the nonlinear simulations.

sharp concentration gradients emerge near the crests, prompting them to grow more rapidly. This confirms the basic instability mechanism familiar from linear stability theory of the pure morphological case.

With an imposed flow of $U = 50$, the interface is seen to be less unstable, cf. the interfacial shapes depicted in figure 17, as well as the overall concentration field shown in figure 18. For the present values of M, k and R, and an externally imposed flow of $U = 50$, linear stability theory predicts a dominant mode with between three and four wavelengths in the computational domain. This is once again confirmed by the nonlinear simulation, which now exhibits four crests. These crests clearly migrate in the downstream direction. However, as predicted by linear theory, the propagation velocity is several orders of magnitude smaller than the externally imposed flow velocity.

4.3.2. *Source and sink flow*

The final configuration to be investigated is that of a source/sink pair in the melt, cf. figure 19. Again the flow is potential in nature, which distinguishes it from earlier analyses such as the stagnation-point flow studied theoretically by Brattkus & Davis (1988*b*). Employing a boundary layer approximation, those authors find that the velocity component normal to the interface has a destabilizing influence. Specifically, the flow is found to destabilize long waves. The authors furthermore observe unstable perturbations travelling against the direction of the flow. A further, more recent theoretical study by Cummings *et al.* (1999) addresses the effects of an irrotational stagnation point flow on an isolated parabolic dendrite. The authors assume the interface to be locally flat at the tip of the dendrite. Their linear stability analysis, which excludes the effect of surface energy, shows the interface to be unstable.

The accompanying experiments in part 1 indicate that a stagnation-point flow in a Hele-Shaw cell initially has a stabilizing influence, due to the convective heat transport of the injected fluid, which impinges on the interface and melts it back. This effect

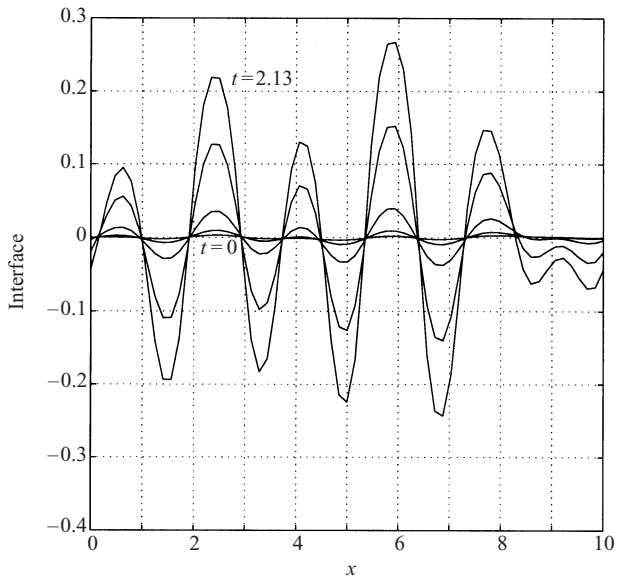

FIGURE 15. Interfacial evolution for $M = 100$, $k = 0.1$ and $R = 0.04$, in the absence of flow. Even though the initial perturbation had only five crests, for longer times we observe the growth of six crests. This is in agreement with the results from linear stability theory, which predicts the largest amplification rate for mode six.

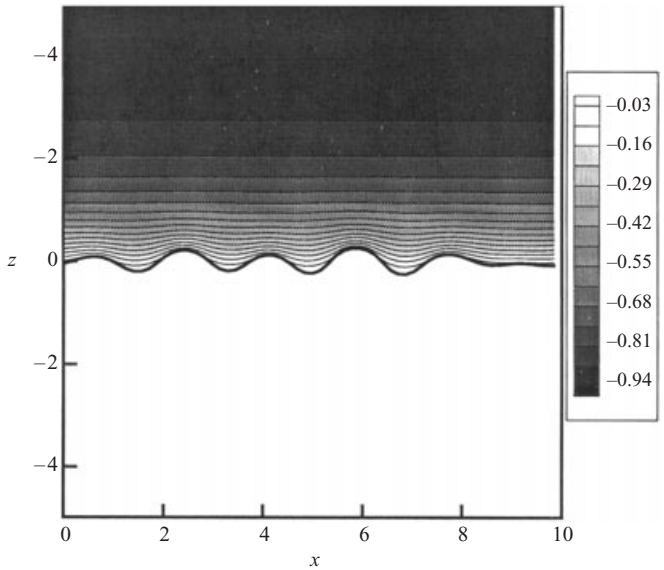

FIGURE 16. Overall concentration field at the final time $t = 2.13$ for $M = 100$, $k = 0.1$ and $R = 0.04$, in the absence of flow. Steeper gradients are seen to form near the crests, while milder gradients emerge in the troughs.

cannot be captured by the present simulations, as we impose the frozen temperature approximation, which does not permit the convective transport of excess heat. After the initial transients settle down, in part 1 the interface is observed to grow more rapidly than in the case of no flow. For weak source flows, they furthermore find that the evolving cells tilt against the direction of the flow, whereas for stronger source flows the cells grow perpendicularly to the initially planar interface.

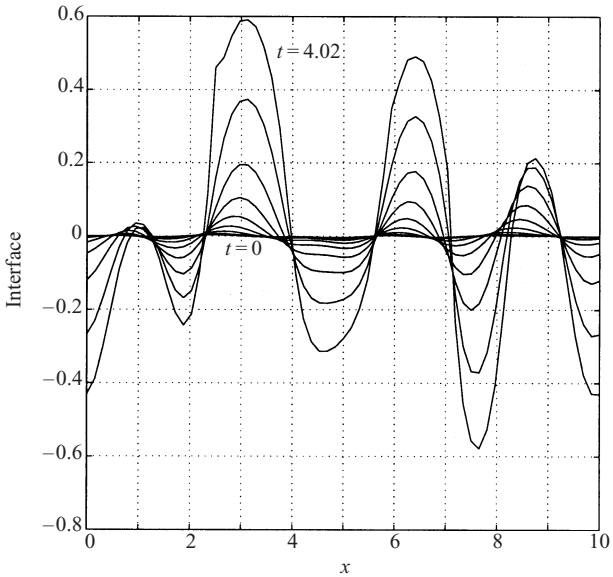

FIGURE 17. Interfacial evolution for $M = 100$, $k = 0.1$, $R = 0.04$ and a uniform flow of $U = 50$. The initial perturbation again is as shown in figure 14. Now only four crests are seen to grow to larger amplitude, due to a further shift of the highest amplification rates to longer waves. At the same time, the growing peaks can be seen to propagate slowly in the direction of the externally imposed flow.

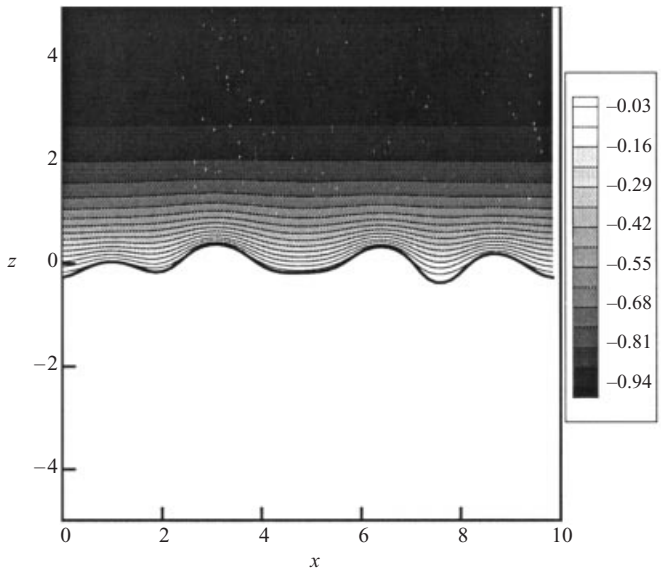

FIGURE 18. Overall concentration field at the final time $t = 3.79$ for $M = 100$, $k = 0.1$, $R = 0.04$ and a uniform flow of $U = 50$. The solidification process remains unstable at this value of U.

In order to analyse the effects of sources and sinks in the flow, we place a source of unit strength at the location $(2.5, 2.5)$, and a sink of equal but opposite strength at $(7.5, 2.5)$. These locations remain fixed in time, i.e. they are unaffected by the pulling of the cell in the $-z$-direction. The source/sink configuration is assumed to extend infinitely in the periodic x-direction. The remaining dimensionless parameters are left at their earlier values, i.e. $M = 100$, $k = 0.1$ and $R = 0.04$. The injected and withdrawn

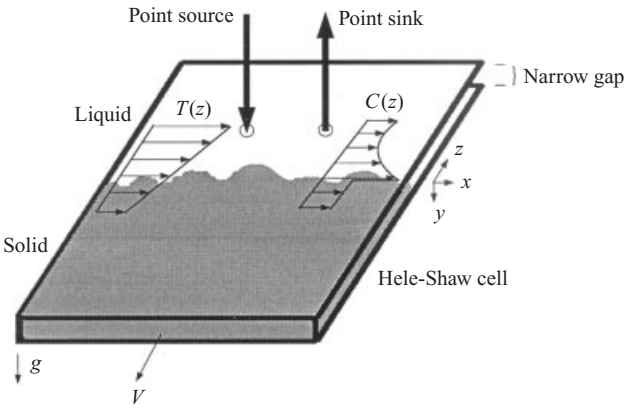

FIGURE 19. Sketch of the source/sink configuration.

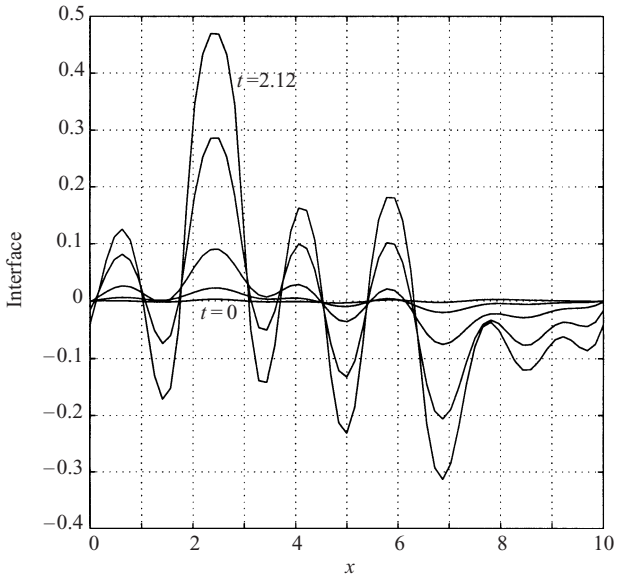

FIGURE 20. Interfacial evolution for $M = 100$, $k = 0.1$ and $R = 0.04$. A source and a sink of unit strength are placed at $(2.5, 2.5)$ and $(7.5, 2.5)$, respectively. The initial perturbation of the interface is identical to that of the above cases with uniform parallel flow. Overall, the unstable solidification interface is observed to approach the source, while it recedes from the sink.

fluid has the temperature corresponding to the local value of the frozen temperature assumption. Its solute concentration is given by the local value of the base state. The initial interfacial shape is identical to the above case for uniform parallel flow.

The temporal evolution of the interface is shown in figure 20. Overall, the interfacial growth is clearly unstable. However, there are pronounced differences between the regions near the source and the sink. The crest nearest to the source quickly outgrows its neighbours and soon becomes dominant. At the same time, the trough closest to the sink evolves more rapidly than those next to it. The interface has a global tendency to accelerate towards the source, and to melt back from the sink. A comparison of figures 20 and 15 shows that the instability grows more rapidly in the presence of the source and sink than in the absence of flow. This observation is in agreement

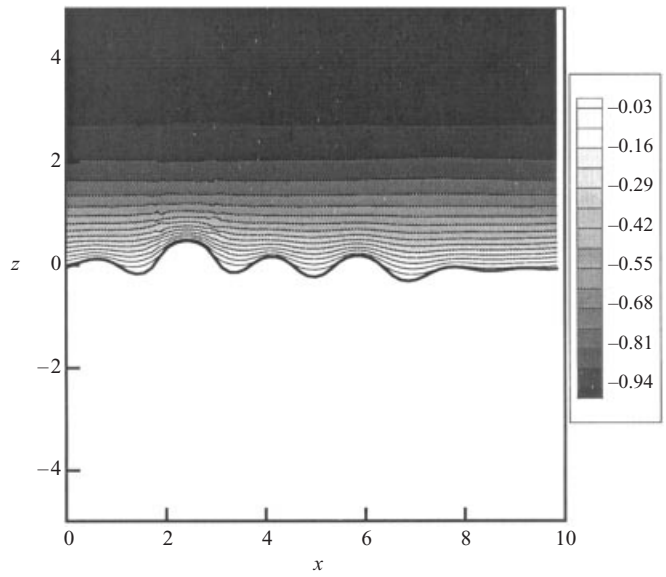

FIGURE 21. Overall concentration field at the final time $t = 2.12$ for $M = 100$, $k = 0.1$ and $R = 0.04$, with the unit strength source and sink placed as described in the text.

with the experiments in part 1, where it was found that, after the initial transients die out, the interfacial instability grows more rapidly when sources and sinks are present. It is also in line with the theoretical work of Brattkus & Davis (1988*b*), who report that a stagnation point flow has a destabilizing influence on the interface. Bühler & Davis (1998) as well as Chen & Davis (1999) consider the morphological instability in the presence of a spatially periodic cellular convection flow in the melt above the interface. This type of flow gives rise to a periodic array of converging and diverging stagnation points along the interface, which is locally similar to the flow generated by the present, periodic array of sources and sinks. If the wavelength of the morphological instability is much shorter than the wavelength of the imposed cellular flow, the authors find that the morphological instability becomes localized near the converging stagnation points. Even though their analysis employs a viscous fluid in contrast to our potential flow, figure 20 indicates such a localization as well. The interfacial waves are seen to grow much more rapidly around the stagnation point near the source than around the stagnation point next to the sink.

Figures 21 and 22 show the overall and perturbation concentration fields, respectively, at the final time $t = 2.12$. The source is seen to convect fluid with low solute concentration towards the interfacial sections closest to it, thereby promoting locally steeper concentration gradients that lead to accelerated growth. The high solute concentration near the interface is transported in the spanwise direction towards the region near the sink, where it results in a relatively mild concentration gradient that inhibits interfacial growth.

5. Discussion and conclusions

Among the main findings from the above linear stability analysis are the observations that a uniform velocity parallel to the interface reduces the growth rate of directional solidification instabilities and shifts the dominant wavelength to somewhat

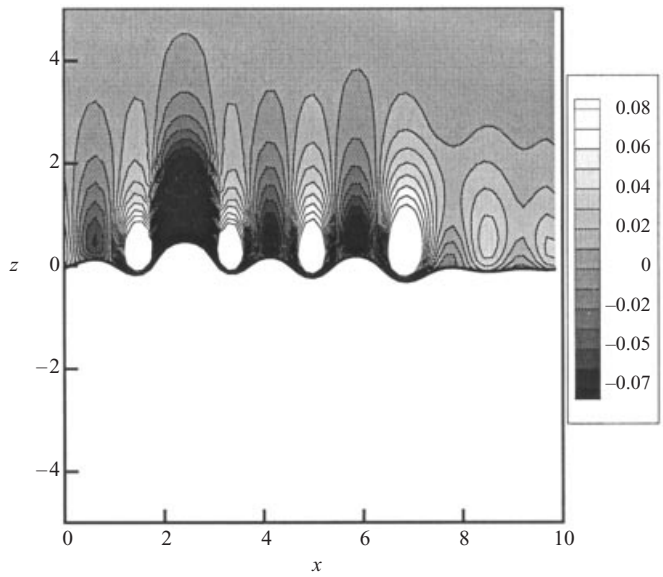

FIGURE 22. Perturbation concentration field at the final time $t = 2.12$ for $M = 100$, $k = 0.1$ and $R = 0.04$, with the unit strength source and sink placed as described in the text. The resulting flow field is seen to enhance the concentration gradient near the source, while reducing it closer to the sink. This provides an explanation for the rapid propagation of the interface towards the source, while it melts away from the sink.

larger values, while causing the unstable waves to propagate slowly in the downstream direction. This behaviour is confirmed by the nonlinear simulations. These observations are in good qualitative agreement with several previous theoretical investigations (cf. Delves 1968, 1971; Coriell *et al.* 1984; Forth & Wheeler 1989; Schulze & Davis 1994, 1995) in the sense that the flow has a stabilizing influence. However, Hobbs & Metzener (1991) find the presence of a constant-velocity flow with a boundary layer profile destabilizing in the long-wave regime. In addition, most of the above mentioned investigations have found interfacial waves travelling in the upstream direction, which is in contrast to the present investigation. This difference can be traced back to the assumption of viscous flow in the earlier analyses, along with the no-slip boundary condition at the solidifying interface.

The accompanying experiments in part 1 show a stabilizing influence of the uniform parallel flow as well. On the other hand, the dominant wavelength appears to be unaffected, and a propagation velocity of the unstable waves is not observed. This is perhaps not very surprising, considering the fact that linear stability theory predicts propagation velocities two to four orders of magnitude smaller than the flow velocity, which may be hard to measure in the experiments. The dominant wavelengths found in part 1 are roughly twice the size predicted by linear theory, while the growth rates are a factor of four lower. For more detailed comparison data, see the discussion in part 1. These considerable differences regarding the dominant wavelengths and growth rates indicate that in the experiments certain mechanisms may be important that are not fully captured by the relatively simple, two-dimensional potential flow model underlying the above linear stability analysis as well as the nonlinear simulations. Foremost among these is the existence of a velocity boundary layer in the melt, next to the solidifying interface. The fact that the no-slip condition has to be satisfied at

this interface results in a local shear flow velocity profile that differs significantly from the potential flow considered theoretically. This, in turn, has a strong influence on the lateral solute transport, and hence on the local shape of the concentration boundary layer next to the interface. The velocity boundary layer thickness will be roughly on the order of the gap width, which in the experiments in part 1 usually is of the same order or even larger than the dominant wavelength. As a result, during their linear growth phase the emerging dendrites in the experiments are located entirely within the velocity boundary layer, i.e. outside the region where the velocity field can be expected to be irrotational. In addition, the solidifying interface in the experiment is not strictly two-dimensional for the relatively large gap width employed in part 1. This is clearly visible in some of the figures presented in part 1 for the late stages of dendritic growth, but even for the early stages characterized by small perturbation levels, the interface is expected to have some curvature in the cross-gap direction. Obviously, this is not accounted for in the stability analysis or the nonlinear simulations. Thus, the potential flow model employed here is seen to be able to predict some qualitatively correct trends, but three-dimensional viscous simulations will be needed in order to obtain quantitatively accurate predictions.

The authors gratefully acknowledge discussions with Professor S. H. Davis of Northwestern University. This work was supported through the NASA Microgravity Program, under grant number NAG8-1240.

REFERENCES

Anderson, Jr, J. D. 1991 *Fundamentals of Aerodynamics*. McGraw-Hill.

Boettinger, W. J., Shechtman, D., Shaefer, R. J. & Biancaniello, F. S. 1984 The effect of rapid solidification velocity on the microstructure of Ag–Cu alloys. *Metall. Trans.* A **15**, 55.

Brattkus, K. & Davis, S. H. 1988*a* Flow-induced morphological instabilities: the rotating disc. *J. Cryst. Growth* **87**, 385.

Brattkus, K. & Davis, S. H. 1988*b* Flow-induced morphological instabilities: stagnation point flows. *J. Cryst. Growth* **89**, 423.

Bühler, L. & Davis, S. H. 1998 Flow-induced changes of the morphological stability in directional solidification: localized morphologies. *J. Cryst. Growth* **186**, 629.

Caroli, B., Caroli, C., Misbah, C. & Roulet, B. 1985*a* Solutal convection and morphological instability in directional solidification of binary alloys. *J. Phys. Paris* **46**, 401.

Caroli, B., Caroli, C., Misbah, C. & Roulet, B. 1985*b* Solutal convection and morphological instability in directional solidification of binary alloys II: effect of the density difference between the two phases. *J. Phys. Paris* **46**, 1657.

Chen, Y.-J. & Davis, S. H. 1999 Directional solidification of a binary alloy into a cellular convective flow: localized morphologies. *J. Fluid Mech.* **395**, 253.

Coriell, S. R., McFadden, G. B., Boisvert, R. F. & Sekerka, R. F. 1984 Effect of a forced Couette flow on coupled convective and morphological instabilities during unidirectional solidification. *J. Cryst. Growth* **69**, 15.

Cummings, L. M., Hohlov, Y. E., Howison, S. D. & Kornev, K. 1999 Two-dimensional solidification and melting in potential flows. *J. Fluid Mech.* **378**, 1.

Dantzig, J. A. & Chao, L. S. 1986 The effect of shear flows on solidification microstructure. *Proc. Tenth US Natl Cong. Appl. Mech.*, p. 249. ASME.

Dantzig, J. A. & Chao, L. S. 1990 Fluid flow and microstructure development. *Proc. Intl Symp. on Solidification Processes*, p. 12.

Davis, S. H. 1990 Hydrodynamic interactions in directional solidification. *J. Fluid Mech.* **212**, 241.

Davis, S. H. 1993 Effects of flow on morphological stability. In *Handbook of Crystal Growth – Fundamentals – Transport and Stability*. North-Holland.

Delves, R. T. 1968 Theory of stability of a solid–liquid interface during growth from stirred melts. *J. Cryst. Growth* **3**, 562.

Delves, R. T. 1971 Theory of stability of a solid–liquid interface during growth from stirred melts. II. *J. Cryst. Growth* **8**, 13.

Forth, S. A. & Wheeler, A. A. 1989 Hydrodynamic and morphological stability of the unidirectional solidification of a freezing binary alloy: a simple model. *J. Fluid Mech.* **202**, 339.

Forth, S. A. & Wheeler, A. A. 1992 Coupled convective and morphological instability in a simple model of the solidification of a binary alloy, including a shear flow. *J. Fluid Mech.* **236**, 61.

Glicksman, M. E., Coriell, S. R. & McFadden, G. B. 1986 Interactions of flows with crystal–melt interface. *Annu. Rev. Fluid Mech.* **18**, 307.

Gottlieb, D. & Orszag, S. A. 1977 *Numerical Analysis of Spectral Methods.* SIAM.

Hobbs, A. K. & Metzener, Ph. 1991 Long-wave instabilities in directional solidification with remote flow. *J. Cryst. Growth* **112**, 539.

Horne, R. N. & Rodriguez, F. 1983 Dispersion in tracer flow in fractured geothermal systems. *Geophys. Res. Lett.* **10**, 289.

Hurle, D. T. J. 1969 Interface stability during solidification of a stirred binary-alloy melt. *J. Cryst. Growth* **5**, 162.

Hurle, D. T. J. 1977 Control of diameter in Czochralski and related crystal growth techniques. *J. Cryst. Growth* **42**, 473.

Langer, J. S. 1980 Instabilities and pattern formation in crystal growth. *Rev. Mod. Phys.* **52**, 1.

Lele, S. K. 1992 Compact finite difference schemes with spectral-like resolution. *J. Comput. Phys.* **103**, 16.

Mullins, W. W. & Sekerka, R. F. 1964 Stability of a planar interface during solidification of a dilute binary alloy. *J. Appl. Phys.* **35**, 444.

Petitjeans, P., Chen, C.-Y., Meiburg, E. & Maxworthy, T. 1999 Miscible quarter five-spot displacements in a Hele-Shaw cell and the role of flow-induced dispersion. *Phys. Fluids* **11**, 1705.

Rutter, J. W. & Chalmers, B. 1953 *Can. J. Phys.* **31**, 15.

Schulze, T. P. & Davis, S. H. 1994 The influence of oscillatory and steady shears on interfacial stability during directional solidification. *J. Cryst. Growth* **143**, 317.

Schulze, T. P. & Davis, S. H. 1995 Shear stabilization of morphological instability during directional solidification. *J. Cryst. Growth* **149**, 253.

Schulze, T. P. & Davis, S. H. 1996 Shear stabilization of a solidifying front: weakly nonlinear analysis in a longwave limit. *Phys. Fluids* **8**, 2319.

Sekerka, R. F. 1968 Morphological stability. *J. Cryst. Growth* **3**, 71.

Tong, X., Beckermann, C. & Karma, A. 2000 Velocity and shape selection of dendritic crystals in a forced flow. *Phys. Rev.* E **61**, R49.

Tonhardt, R. & Amberg, G. 1998 Phasefield simulation of dendritic growth in a shear flow. *J. Cryst. Growth* **194**, 406.

Tonhardt, R. & Amberg, G. 2000 Dendritic growth of randomly oriented nuclei in a shear flow. *J. Cryst. Growth* **213**, 161.

Trivedi, R., Sekhar, J. A. & Seetharaman, V. 1989 *Met. Trans.* A **20a**, 769.

Wray, A. A. 1991 Minimal storage time-advancement schemes for spectral methods. *Preprint.*

Zhang, M. & Maxworthy, T. 2002 The interactive dynamics of flow and directional solidification in a Hele-Shaw cell. Part 1. Experimental investigation of parallel shear flow. *J. Fluid Mech.* **470**, 247.